Published in "Tetrahedron Letters 53(7): 794-799, 2011"
which should be cited to refer to this work.

Magnetic criteria of aromaticity in a benzene cation and anion: how does the Jahn–Teller effect influence the aromaticity?

Ljubica Andjelković [a], Marko Perić [a], Matija Zlatar [a], Sonja Grubišić [a], Maja Gruden-Pavlović [b,*]

[a] Center for Chemistry, IHTM, University of Belgrade, Studentski Trg 12-16, 11001 Belgrade, Serbia
[b] Department of Chemistry, University of Fribourg, Chemin du Musée 9, CH 1700 Fribourg, Switzerland

The aromatic/antiaromatic behavior of the Jahn–Teller (JT) active benzene cation and anion has been investigated using Density Functional Theory (DFT) calculations of Nuclear Independent Chemical Shifts (NICS) and magnetic susceptibility. NICS parameters have been scanned along the Intrinsic Distortion Path (IDP) for the benzene cation showing antiaromaticity which decreases with increasing deviation from D_{6h} to D_{2h} symmetry. Changes in NICS values along the IDP from D_{6h} to C_{2v} in the benzene anion revealed non-aromatic character.

Aromaticity and the Jahn–Teller effect[1,2] are concepts of crucial importance in physical organic chemistry, and they have been very useful in the characterization and interpretation of the structure, stability, and reactivity of many molecules. The Hückel Molecular Orbital (MO) theory proposes that species with 4n+2 π electrons are aromatic, whereas structures with 4n π electrons are defined as antiaromatic.[3,4] Structures with 4n+1 π electrons with unpaired electrons in degenerate π orbitals are Jahn–Teller active species, and are supposed to show antiaromaticity.[5,6]

Although the above mentioned Hückel rules of aromaticity, based on the number of electrons in π MOs, are very appealing due to their simplicity, they actually neither quantify nor give physical explanation of this effect. Because of the importance of aromaticity, there have been many attempts to rationalize it and to derive a universal quantitative measure of it.[7–10] Features of aromatic compounds include low reactivity in addition reactions, high electrophilic aromatic substitution/addition ratios of reactivity, elevated energy of hydrogenation, typical values of bond lengths which are intermediate between normal single and double bonds, planarity and specific magnetic properties of aromatic rings: proton chemical shifts, magnetic susceptibility exaltation, nucleus-independent chemical shifts (NICS), and ring current plots.[11–16] Each of these properties can be used to probe the aromaticity of a molecule, though unfortunately, they do not need to be consistent with each other. Computed NICS indices are presently the most widely used and are a very efficient tool for the exploration of this phenomenon. The diamagnetic and paramagnetic effects of the ring currents associated with aromatic and antiaromatic features (i.e., shielding and deshielding of nuclei) can be determined according to the calculated NICS index. Negative NICS values in interior positions of rings indicate the presence of induced diatropic ring currents, or aromaticity, whereas positive values denote paratropic ring currents and antiaromaticity. The more negative the NICS values, the more aromatic the rings are. NICS parameters can be computed at selected points inside or around molecules, typically at ring centers and above. NICS values calculated at the geometrical center of the ring are denoted as NICS(0).[17] Similarly, NICS values at 1 Å above the perpendicular plane of the rings are defined as NICS(1), and the $NICS(1)_{zz}$ tensor component has been presented to provide better insight of the overall molecular magnetic properties. It was suggested that this latter quantity gives the best measure of aromaticity among the different NICS related definitions.[18] NICS(0) and $NICS(1)_{zz}$ values describe rather different effects. It is likely that $NICS(1)_{zz}$ values account mainly for the π aromaticity effect, while NICS(0) results better reflect both the σ and π aromaticity or antiaromaticity effects.

The Jahn–Teller theorem states that a molecule with a degenerate electronic state distorts along non-totally symmetric vibrational coordinates. This removes the degeneracy and lowers the energy.[1,2] Nowadays, this definition is generalized to include all the effects arising due to the coupling of electron distribution with nuclear movements in a molecule.[2] Thus, Jahn–Teller (JT), or vibronic coupling type distortions include proper JT distortions of molecules in a degenerate electronic state,[1] pseudo JT (PJT)

* Corresponding author at present address: Faculty of Chemistry, University of Belgrade, Studentski Trg 12-16, 11001 Belgrade, Serbia. Tel.: +381 113336754; fax: +381 112635425.
E-mail address: gmaja@chem.bg.ac.rs (M. Gruden-Pavlović).

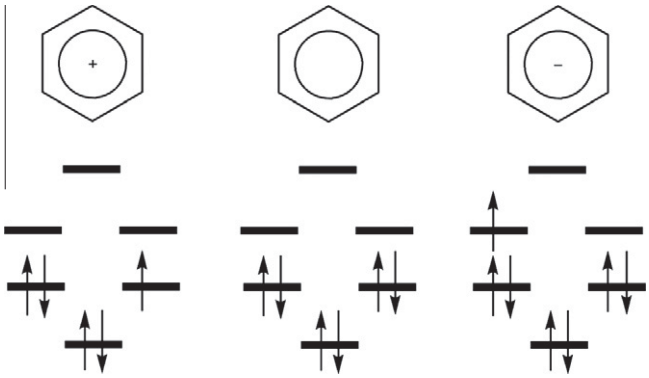

Figure 1. Molecules studied in this work; simple molecular orbital scheme.

distortions in nondegenerate electronic states,[2] and Renner–Teller (RT) distortions in linear systems.[19] Typical examples of molecules prone to the proper JT effect are the benzene cation ($C_6H_6^+$) and benzene anion ($C_6H_6^-$). Recently, the JT distortion in these molecules was analyzed in detail using the Intrinsic Distortion Path (IDP) method.[20,21] The basis of this method is to represent the distortion along the minimal energy path from the high symmetry (HS) nuclear arrangement to the lower symmetry (LS) energy minimum conformation projecting the geometry of the system on the normal modes of the distorted configuration.[20–23]

The aim of the present work was to determine the influence of the JT distortion on antiaromaticity in $C_6H_6^+$ and $C_6H_6^-$ (Fig. 1). More specifically, we would like to answer the question whether the JT effect can be regarded as the origin of the antiaromaticity in these systems. For this purpose, NICS values for $C_6H_6^+$ and $C_6H_6^-$ were calculated along the relevant particular path of distortion, the IDP path, and evaluation of their magnetic susceptibility and anisotropy was undertaken. A discussion on whether the loss or gain of antiaromaticity occurs gradually along the IDP or suddenly at a certain point on the adiabatic potential energy surface will help to gain insight into the relationship between the vibronic coupling and aromaticity.

The benzene molecule, C_6H_6, with D_{6h} nuclear arrangement has a double degenerate HOMO, e_{1g}, and a double degenerate LUMO, e_{2u}. Hence, both $C_6H_6^+$ and $C_6H_6^-$, with 4n+1 π electrons are JT unstable and prefer the conformation of lower symmetry.

$C_6H_6^+$ has an $^2E_{1g}$ ground electronic state in regular hexagonal nuclear configuration, and D_{6h} point group, with three electrons in the doubly degenerate orbital. According to group theory, the distortion coordinate is e_{2g}. Due to the JT effect, the descent in symmetry goes to D_{2h}.[†] $C_6H_6^-$ has an $^2E_{2u}$ ground electronic state in a conformation that belongs to the D_{6h} point group, with one electron in the doubly degenerate orbital. As in the case of $C_6H_6^+$, the distortion coordinate is e_{2g}, thus very similar distortion is expected for $C_6H_6^-$, with a descent in symmetry to the D_{2h} point group. However, DFT calculations showed significant differences between the electronic structure of $C_6H_6^+$ and $C_6H_6^-$.[20] Due to the pseudo Jahn–Teller (PJT) coupling of the ground π^* electronic state with the excited σ^* state in $C_6H_6^-$, the out-of-plane C_{2v} conformation is found to be the global minimum on the potential energy surface. The C_{2v} geometry obtained is a consequence of both proper JT and PJT distortion. The calculated JT parameters of $C_6H_6^+$ and $C_6H_6^-$ using a multideterminantal DFT approach[23,26] and the IDP method are given in Table 1, while changes in energies along the IDP are depicted in Figures 2a, 3a and 4a.[20] Note that any geometry along the path is represented by $\vec{R}_X$ in mass weighted generalized coordinates relative to the LS energy minimum; and for the HS point, $\vec{R}_X = \vec{R}_{JT}$, which is the JT radius. In all cases, on the potential energy profile it is possible to distinguish two regions. In the first region the energy is changing faster, and for D_{6h} to D_{2h} distortion, after 20–30% of the path, most of the E_{JT} is obtained (Figs. 2a and 3a). In the analysis of the D_{6h} to C_{2v} distortion in $C_6H_6^-$ (Fig. 4a), very early along the IDP, ca. after 5% of the path, a strong stabilization of around 500 cm^{-1} is achieved. In the second region the adiabatic energy surface is not flat, and the energy gradually decreases an additional 500 cm^{-1}. In this region distortion is almost completely described with the out-of-plane normal mode.[20] Analysis of the changes of the aromatic character of these JT active molecules along the IDP for $D_{6h}\rightarrow D_{2h}$ distortion for both $C_6H_6^+$ and $C_6H_6^-$, and $D_{6h}\rightarrow C_{2v}$ for $C_6H_6^-$ are shown in Figures 2b, 3b and 4b.

Table 1
Results of the DFT calculations performed to analyze the JT effect in $C_6H_6^+$ and $C_6H_6^-$;[20] JT parameters: the JT stabilization energy, E_{JT}, and the warping barrier, Δ, are given in cm^{-1}, the JT radius, R_{JT}, in $(amu)^{1/2}$Å

	Distortion	E_{JT} (DFT)	E_{JT} (IDP)	Δ	R_{JT}
$C_6H_6^+$	$D_{6h}\rightarrow D_{2h}$	879	857	29.1	0.27
$C_6H_6^-$	$D_{6h}\rightarrow C_{2v}$	1187	1060	46.8	0.62

The benzene molecule is a typical example of a π aromatic system, showing a minimum NICS value at certain distances from the center of the ring plane (Table 2). Magnetic susceptibility data for benzene are presented in Table 3. All calculations of NICS parameters on C_6H_6, performed for comparison purposes, were in good agreement with other theoretical values [NICS(0) = −9.7 ppm].[18]

For both $C_6H_6^+$ and $C_6H_6^-$, NICS values were evaluated at the ring center above the ring plane (0–10 Å) along the IDP path from D_{6h} to D_{2h} structures and the values for the HS and LS points are reported in Table 2. Since the calculation of magnetic properties in species with a degenerate ground state may lead to incorrect results, we calculated NICS values imposing HS (D_{6h}) nuclear arrangement and LS (D_{2h}) symmetry of electron density. NICS values monitored along the path for the $^2B_{2g}$ state in $C_6H_6^+$ and the ^2A_u state in $C_6H_6^-$, which are the minima on the corresponding D_{2h} potential energy surfaces, are presented herein. The results for other states are qualitatively the same.[‡] According to the obtained NICS index (Table 2), $C_6H_6^+$ and $C_6H_6^-$ reveal antiaromatic character, as expected.[6] However, plotted NICS values versus the JT distortion, $\vec{R}_X/\vec{R}_{JT}$, and the distance from the ring center (Figs. 2b and 3b) give a more detailed picture. Aromaticity favors bond equalization while antiaromaticity leads to bond alternation. Removing or adding an electron to the benzene molecule causes non-totally symmetric electron density in the high symmetry, D_{6h} point group, while bond distances remain the same. Due to the non-totally symmetric electron density, $C_6H_6^+$ and $C_6H_6^-$, in D_{6h}, possess strong antiaromatic character. Near the point of electron degeneracy the HOMO–LUMO gap is significantly small, hence NICS parameters have large values in the first region of the distortion path (Figs. 2b and 3b). Although the JT distortion leads to bond unequalization, our results reveal lowering of

[†] The irreducible representations (irreps) of the non-totally symmetric JT active modes must belong to the same representation as the symmetric direct product of the components of the degenerate electronic state. The point group of the LS minimum energy conformation is defined by the requirement that the irreps of the active modes become totally symmetric upon descent in symmetry and the application of the epikernel principle. [2,24,25]

[‡] Due to the JT effect, the doubly degenerate electronic state splits into two states with different geometries at the stationary points, one that becomes a minimum on the potential energy surface, while the other is a transition state for the process of pseudorotation around the JT high symmetry cusp; the energy difference between them is the warping barrier Δ. [2] For the D_{6h} to D_{2h} distortion in $C_6H_6^+$ these are elongated $^2B_{2g}$ (minimum) and compressed $^2B_{3g}$ (transition state), and for D_{6h} to D_{2h} distortion in C_6H_6 these are elongated ^2Au (minimum) and compressed $^2B_{1u}$ (transition state)[20]; Δ is rather small for the present cases, Table 1.

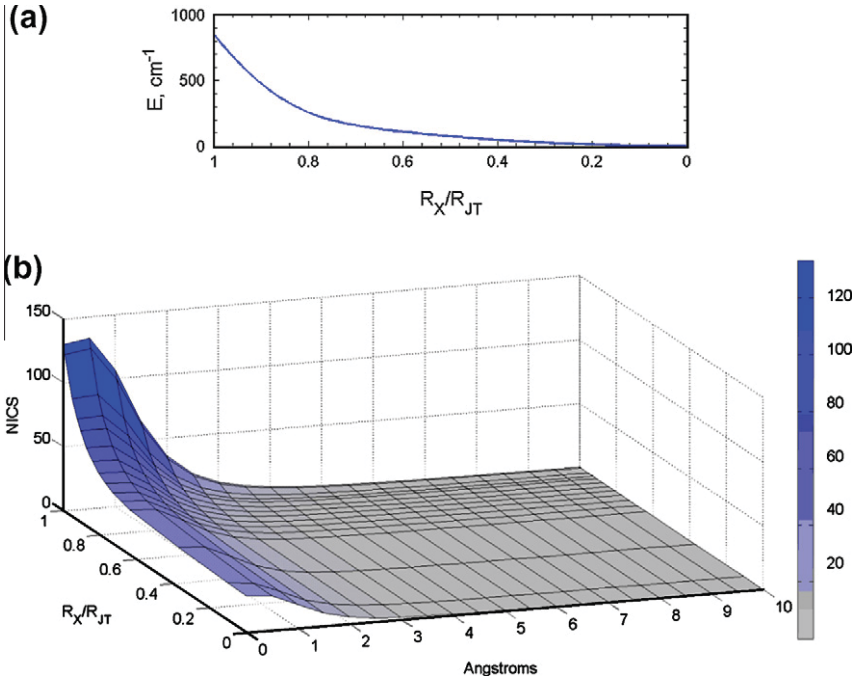

Figure 2. (a) Changes in energy, IDP model; (b) Schematic plots of the NICS values along the IDP for the benzene cation (D_{6h} to D_{2h}), $^2B_{2g}$ electronic state.

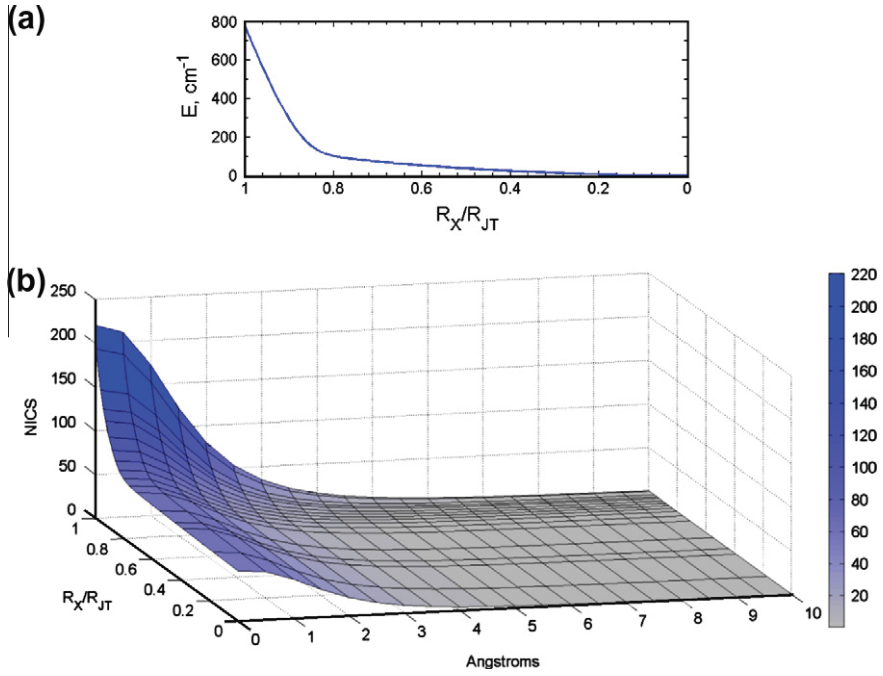

Figure 3. (a) Changes in energy, IDP model; (b) Schematic plots of the NICS values along the IDP for the benzene anion (D_{6h} to D_{2h}), ^2A_u electronic state.

antiaromatic behavior along the IDP. The forces responsible for removing orbital degeneracy lead to enhancement of the HOMO–LUMO gap.

Values of molar magnetic susceptibility, magnetic anisotropy, and the z-component of the magnetic tensor for the studied molecules, at their HS and LS conformations, are given in Table 3. In comparison to benzene, $C_6H_6^+$ in D_{6h} point group has large positive magnetic susceptibility data, while in the global minimum, D_{2h} symmetry, these values become slightly negative. In the case of $C_6H_6^-$, the z-component of the magnetic tensor has a large positive value for a molecule in HS conformation and becomes negative after the first descent in symmetry. The large negative magnetic anisotropy value for the benzene anion in D_{2h} symmetry cannot be an indicator for aromatic character since the x-component of the magnetic tensor has a large positive value, while the y- and z-components have small negative values (χ_{xx} = 192.7 cgs-ppm, χ_{yy} = −27.1 cgs-ppm, χ_{zz} = −23.7 cgs-ppm).

Although D_{6h} and D_{2h} species are planar, the global minimum of $C_6H_6^-$, C_{2v} structure with $^2A_1$ electronic state, is slightly puckered, thus we have calculated NICS parameters at the center, above

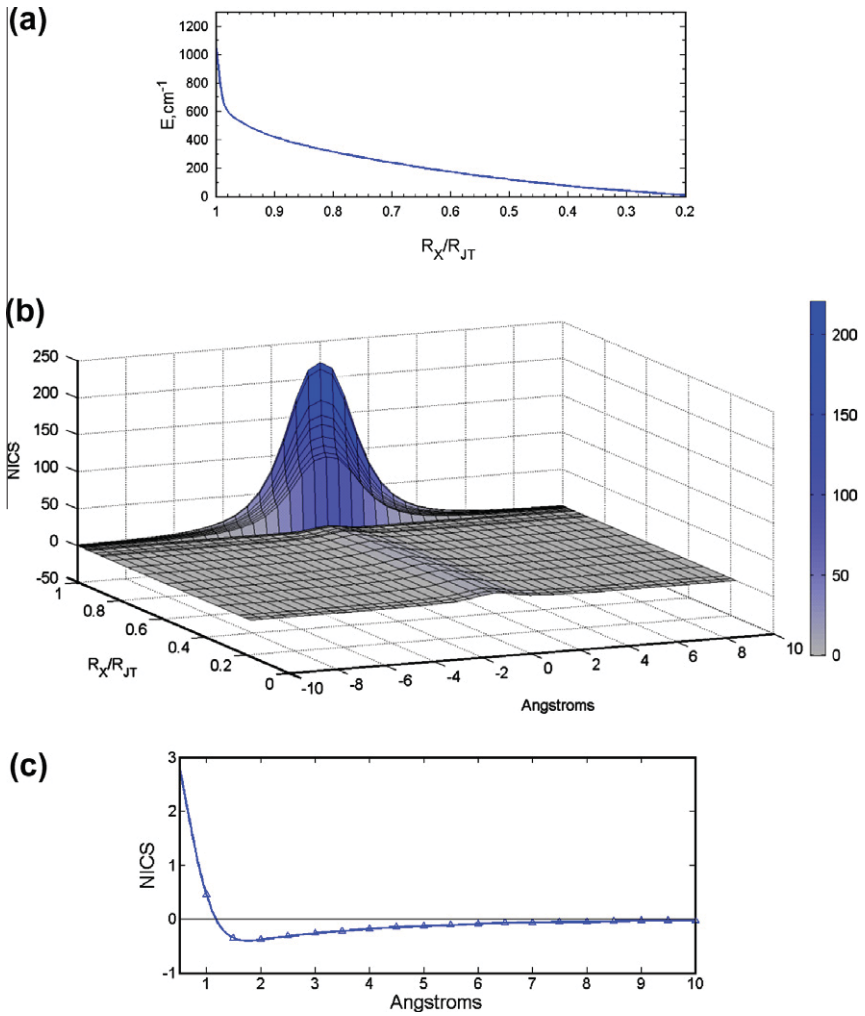

Figure 4. (a) Changes in energy, IDP model; (b) Schematic plots of the NICS values along the IDP for the benzene anion (D_{6h} to C_{2v}), $^2A_1$ electronic state; (c) Schematic plot of the NICS values from the ring center up to 10 Å above the ring following an axis perpendicular to the ring plane, at $R_X/R_{JT} = 0.97$.

Table 2
Calculated NICS values for C_6H_6, $C_6H_6^+$ and $C_6H_6^-$ at HS and LS geometries; NICS(0), NICS(1) and $NICS_{zz}(1)$ are given in ppm

	Geometry	Electronic state	NICS(0)	NICS(1)	$NICS_{zz}(1)$
C_6H_6	D_{6h}	$^1A_{1g}$	−7.9	−10.1	−29.0
$C_6H_6^+$	D_{6h}	$^2B_{2g}$	130.2	106.2	322.1
	D_{2h}	$^2B_{2g}$	28.3	18.5	59.1
$C_6H_6^-$	D_{6h}	^2A_u	220.3	172.6	502.7
	D_{2h}	^2A_u	57.3	45.0	129.2
	C_{2v}	$^2A_1$	9.7	5.4	17.9

Table 3
Magnetic susceptibility data for C_6H_6, $C_6H_6^+$ and $C_6H_6^-$ at HS and LS geometries; χ_M, $\Delta\chi$, and χ_{zz} are given in cgs-ppm

	Geometry	Electronic state	χ_M	$\Delta\chi$	χ_{zz}
C_6H_6	D_{6h}	$^1A_{1g}$	−56.1	−64.9	−99.4
$C_6H_6^+$	D_{6h}	$^2B_{2g}$	75.1	293.0	270.5
	D_{2h}	$^2B_{2g}$	−16.1	−9.8	−22.6
$C_6H_6^-$	D_{6h}	^2A_u	286.2	818.2	831.7
	D_{2h}	^2A_u	47.3	−106.6	−23.7
	C_{2v}	$^2A_1$	−46.3	23.4	−30.7

and below the average ring plane (−10 to 10 Å). The results obtained from D_{6h} toward distorted C_{2v} structure, considering the combined JT/PJT effect, are given in Table 2. Following NICS values along the IDP, from the HS point to C_{2v} minimum energy conformation, two regions could be distinguished. In the first 3% of the path the JT effect dominates, the molecule stays planar and NICS values decrease fast but smoothly, similar to the previously described case. In the second region, where the distortion is almost completely described by the out-of-plane vibration,[20] decreasing of NICS values is abrupt. At the point $R_X/R_{JT} = 0.97$ an almost step-like change in the NICS values occurs. At this point NICS parameters change from low positive to low negative values as the distance from the ring plane increases (Fig. 4b and c), revealing the non-aromatic character.[27] Explanation for this abrupt change of NICS values is associated with mixing of the ground π^* state with the first excited σ^* state at a certain point, which leads to discontinuity in the values. It should be pointed out that from the same point, PJT mixing becomes very important, and determines the overall puckered structure.

Magnetic susceptibility data for $C_6H_6^-$ for the distortion caused by combined JT/PJT effects are presented in Table 3. Observing reduction of symmetry from D_{6h} to C_{2v} (global minimum on the potential energy surface) the magnetic susceptibility data have almost the same trend as in the $C_6H_6^+$ ion.

Aromaticity and the Jahn–Teller type distortions are two deeply connected concepts, although this is not very often addressed. While the physical nature of aromaticity is still not completely understood, there is no ambiguity in defining the JT effect, which is the only source of spontaneous distortion of any polyatomic

system,[2] although difficulties in its quantification, especially by experiment still exist. The JT distortion often leads to unequal bond lengths, and antiaromaticity of JT species can be intuitively predicted. Monitoring the changes in NICS values for $C_6H_6^+$ and $C_6H_6^-$ along the IDP path indicate that antiaromaticity decreases with increasing deviation from D_{6h} to D_{2h} point group. Thus, the Jahn–Teller effect is not a source of antiaromaticity, and rather is the mechanism of lowering it. $C_6H_6^-$ adopts a non-planar conformation in its global minimum as a consequence of the combined JT/PJT effect,[20] thus avoiding undesirable antiaromaticity. However, if we compute NICS values only in D_{6h} structure and C_{2v} global minimum conformation, wrong conclusions can be made and antiaromatic character could be determined. The full NICS profile along the IDP shows non-aromatic behavior. These results suggest that without analyzing details on how NICS values change along the distortion path, chemically important features could be lost. The IDP method gives direct insight on microscopic origin, mechanism and consequences of distortion and further work along this line could hopefully lead to some more general trends. In the case of antiaromatic systems such analysis may help to understand if antiaromaticity is just a useful concept or if there is some physical reasoning behind it.

1. Computational details

The structures of $C_6H_6^+$and $C_6H_6^-$ were optimized by DFT calculations using the Amsterdam Density Functional program package, ADF2009.01.[28–30] The local density approximation (LDA) characterized by the Vosko-Willk-Nusair (VWN)[31] parameterization was used for the symmetry-constrained geometry optimizations. An all electron Triple-zeta Slater-type orbitals (STO) plus one polarization function (TZP) basis set was used for all atoms. Analytical harmonic frequencies[32,33] were calculated and in all cases the global minimum was confirmed by the absence of imaginary frequency modes.

Calculations of NICS values and magnetic susceptibility data were performed at the B3LYP/6-311+G* level of theory using the Gaussian 09W program package.[34–37] NICS parameters were calculated for ghost atoms located at the center of C_6H_6, $C_6H_6^+$ and $C_6H_6^-$. In order to obtain the full profile of aromatic/antiaromatic behavior of the investigated molecules, calculations of NICS parameters were performed from 0 to 10 Å, in steps of 0.5 Å, along the IDP.[20]

In addition to the nucleus-independent chemical shifts, mean molar magnetic susceptibility (χ_M) and molar magnetic anisotropy ($\Delta\chi$) became important tools to prove the term of aromaticity. The tensor normal to the aromatic ring (χ_{zz}) is much larger than the average of other tensors, thus the aromatic compounds have large negative magnetic anisotropy (Eqs. 1 and 2).

$$\chi_M = \frac{\chi_{xx} + \chi_{yy} + \chi_{zz}}{3} \tag{1}$$

$$\Delta\chi = \chi_{zz} - \frac{\chi_{zz} + \chi_{zz}}{2} \tag{2}$$

2. Intrinsic distortion path (IDP)

In the IDP model,[20,21] the geometry of the LS energy minimum obtained by DFT calculations, in this particular case D_{2h} for $C_6H_6^+$ and D_{2h} or C_{2v} for $C_6H_6^-$, was chosen to be the origin of the configuration space, $\vec{R}_{LS} = 0$. Every point on the potential energy surface can be represented by a 3N dimensional vector, N being the number of atoms, $\vec{R}_X$, using mass-weighted generalized coordinates relative to the origin. Within the harmonic approximation it is possible to express $\vec{R}_X$ as a linear combination of N_{a1} totally symmetric normal coordinates in the LS confirmation:

$$\vec{R}_x = \sum_{k=1}^{N_{a1}} \omega_{Xk}\vec{Q}_k \tag{3}$$

where ω_{Xk} are weighting factors which represent the contribution of the displacements along the different totally symmetric normal coordinates to $\vec{R}_X$; $\vec{Q}_X$ are mass-weighted totally symmetric normal coordinates, which are the eigenvectors of the Hessian, obtained from the DFT frequency calculations in the LS minimum energy conformation. The corresponding eigenvalues are λ_k.

The energy of the nuclear configuration $\vec{R}_X$, E_X, relative to the LS energy minimum is expressed as the sum of the energy contributions of the totally symmetric normal modes:

$$E_X = \sum_{k=1}^{N_{a1}} E_K = \frac{1}{2}\sum_{k=1}^{N_{a1}} \omega_{Xk}^2 \vec{Q}_k^2 \lambda_k \tag{4}$$

The force at any given point (X), $\vec{F}_{Xk}$ is defined as a derivate of the energy over Cartesian coordinates and in the HS point indicates the main driving force for the JT distortion. The total force is represented as a vector sum of the individual forces:

$$\vec{F}_{Xtot} = \sum_{k=1}^{N_{a1}} \vec{F}_{Xk} = \sum_{k=1}^{N_{a1}} \omega_{Xk}\lambda_k \mathbf{M}^{1/2}\vec{Q}_k \tag{5}$$

where **M** is a diagonal $3N \times 3N$ matrix with atomic masses in triplicate as elements ($m_1,m_1,m_1,m_2,\ldots,m_n$), and enable calculation of the IDP exactly from the HS to the LS point.

Acknowledgments

This work was supported by the Serbian Ministry of Science (Grant No. 172035) and the Swiss National Science Foundation.

References and notes

1. Jahn, H. A.; Teller, E. *Proc. R. Soc. London, Ser. A* **1937**, *161*, 220.
2. Bersuker, I. B. *The Jahn–Teller Effect*; Cambridge University Press, 2006.
3. Hückel, E. *Z. Phys.* **1931**, *70*, 204.
4. Hückel, E. *Z. Phys.* **1932**, *78*, 628.
5. Allen, A. D.; Tidwell, T. T. *Chem. Rev.* **2001**, *101*, 1333.
6. Tsipis, A. C. *Phys. Chem. Chem. Phys.* **2009**, *11*, 8244.
7. von Ragué Schleyer, P. *Chem. Rev.* **2001**, *101*, 1115.
8. Garrat, P. J. *Aromaticity*; Wiley: New York, 1986.
9. Minkin, V. I.; Glukhovtsev, M. N.; Simkin, B. Y. *Aromaticity and Antiaromaticity: Electronic and Structural Aspects*; Wiley: New York, 1994.
10. von Ragué Schleyer, P.; Jiao, H. *Pure Appl. Chem.* **1996**, *68*, 209.
11. Chen, Z.; Wannere, C. S.; Corminboeuf, C.; Puchta, R.; von Ragué Schleyer, P. *Chem. Rev.* **2005**, *105*, 3842.
12. von Ragué Schleyer, P.; Manoharan, M.; Wang, Z.-X.; Kiran, B.; Jiao, H.; Puchta, R.; van Eikema Hommes, N. J. R. *Org. Lett.* **2001**, *3*, 2465.
13. Katritzky, A. R.; Jug, K.; Oniciu, D. C. *Chem. Rev.* **2001**, *101*, 1421.
14. Krygowski, T. M.; Cyrański, M. K. *Chem. Rev.* **2001**, *101*, 1385.
15. De Proft, F.; Geerlings, P. *Chem. Rev.* **2001**, *101*, 1451.
16. Gomes, J. A. N. F.; Mallion, R. B. *Chem. Rev.* **2001**, *101*, 1349.
17. n Ragué Schleyer, P.; Maerker, C.; Dransfeld, A.; Jiao, H.; van Eikema Hommes, N. J. R. *J. Am. Chem. Soc.* **1996**, *118*, 6317.
18. Corminboeuf, C.; Heine, T.; Seifert, G.; von Ragué Schleyer, P.; Weber, J. *Phys. Chem. Chem. Phys.* **2004**, *6*, 273.
19. Renner, R. *Z. Phys. A* **1934**, *92*, 172.
20. Gruden-Pavlovic, M.; García-Fernández, P.; Andjelkovic, Lj.; Daul, C.; Zlatar, M. *J. Phys. Chem. A* **2011**, *115*, 10801.
21. Zlatar, M.; Brogg, J. P.; Tschannen, A.; Gruden-Pavlovic, M.; Daul, C. In *Vibronic Interactions and the Jahn–Teller Effect, Progress in Theoretical Chemistry and Physics*; Atanasov, M., Daul, C., Tregenna-Piggott, P. L. W., Eds.; Springer, 2012; Vol. 23, pp 25–38.
22. Zlatar, M.; Gruden-Pavlović, M.; Schläpfer, C.-W.; Daul, C. *J. Mol. Struct. THEOCHEM* **2010**, *954*, 86.
23. Zlatar, M.; Schläpfer, C.-W.; Daul, C. In *The Jahn–Teller-Effect Fundamentals and Implications for Physics and Chemistry, Springer Series in Chemical Physics*; Köppel, H., Yarkoni, D. R., Barentzen, H., Eds.; Springer, 2009; Vol. 97, pp 131–165.
24. Ceulemans, A.; Vanquickenborne, L. G. *Struct. Bond.* **1989**, *71*, 125.
25. Ceulemans, A.; Beyens, D.; Vanquickenborne, L. G. *J. Am. Chem. Soc.* **1984**, *106*, 5824.
26. Bruyndonckx, R.; Daul, C.; Manoharan, P. T.; Deiss, E. *Inorg. Chem.* **1997**, *36*, 4251.

27. Jiménez-Halla, J. O. C.; Matito, E.; Robles, J.; Solà, M. *J. Organomet. Chem.* **2006**, *691*, 4359.
28. ADF2009, SCM, Theoretical Chemistry, Vrije Universiteit, Amsterdam, The Netherlands, http://www.scm.com.
29. Guerra, C. F.; Snijders, J. G.; te Velde, G.; Baerends, E. *J. Theor. Chem. Acc.* **1998**, *99*, 391.
30. te Velde, G.; Bickelhaupt, F. M.; van Gisbergen, S. J. A.; Guerra, C. F.; Baerends, E. J.; Snijders, J. G.; Ziegler, T. *J. Comput. Chem.* **2001**, *22*, 931.
31. Vosko, S.; Wilk, L.; Nusair, M. *Can. J. Phys.* **1980**, *58*, 1200.
32. Bérces, A.; Dickson, R. M.; Fan, L.; Jacobsen, H.; Swerhone, D.; Ziegler, T. *Comput. Phys. Commun.* **1997**, *100*, 247.
33. Jacobsen, H.; Bérces, A.; Swerhone, D.; Ziegler, T. *Comput. Phys. Commun.* **1997**, *100*, 263.
34. Gaussian 09, Revision A.1, Frisch, M. J.; Trucks, G. W.; Schlegel, H. B.; Scuseria, G. E.; Robb, M. A.; Cheeseman, J. R.; Scalmani, G.; Barone, V.; Mennucci, B.; Petersson, G. A.; Nakatsuji, H.; Caricato, M.; Li, X.; Hratchian, H. P.; Izmaylov, A. F.; Bloino, J.; Zheng, G.; Sonnenberg, J. L.; Hada, M.; Ehara, M.; Toyota, K.; Fukuda, R.; Hasegawa, J.; Ishida, M.; Nakajima, T.; Honda, Y.; Kitao, O.; Nakai, H.; Vreven, T.; Montgomery, Jr., J. A.; Peralta, J. E.; Ogliaro, F.; Bearpark, M.; Heyd, J. J.; Brothers, E.; Kudin, K. N.; Staroverov, V. N.; Kobayashi, R.; Normand, J.; Raghavachari, K.; Rendell, A.; Burant, J. C.; Iyengar, S. S.; Tomasi, J.; Cossi, M.; Rega, N.; Millam, N. J.; Klene, M.; Knox, J. E.; Cross, J. B.; Bakken, V.; Adamo, C.; Jaramillo, J.; Gomperts, R.; Stratmann, R. E.; Yazyev, O.; Austin, A. J.; Cammi, R.; Pomelli, C.; Ochterski, J. W.; Martin, R. L.; Morokuma, K.; Zakrzewski, V. G.; Voth, G. A.; Salvador, P.; Dannenberg, J. J.; Dapprich, S.; Daniels, A. D.; Farkas, Ö.; Foresman, J. B.; Ortiz, J. V.; Cioslowski, J.; Fox, D. J. Gaussian, Inc., Wallingford CT, 2009.
35. Becke, A. D. *J. Chem. Phys.* **1986**, *84*, 4524.
36. Perdew, J. P.; Yue, W. *Phys. Rev.* **1986**, *33*, 8800.
37. Perdew, J. P. *Phys. Rev.* **1986**, *33*, 8822.